Available online at www.sciencedirect.com
ScienceDirect
Ceramics International 35 (2009) 791–796
CERAMICS INTERNATIONAL
www.elsevier.com/locate/ceramint

Thermal expansion and thermal conductivity of $Sm_xZr_{1-x}O_{2-x/2}$ ($0.1 \leq x \leq 0.5$) ceramics

Zhan-Guo Liu, Jia-Hu Ouyang *, Bai-He Wang, Yu Zhou, Jing Li

Institute for Advanced Ceramics, Department of Materials Science, Harbin Institute of Technology, P.O. Box 433, Harbin 150001, PR China

Received 23 November 2007; received in revised form 12 December 2007; accepted 22 February 2008
Available online 28 June 2008

Abstract

A study was conducted of the effect of additions of samarium oxide on the thermal expansion and thermal conductivity of zirconium oxide for thermal barrier coatings. $Sm_xZr_{1-x}O_{2-x/2}$ ($0.1 \leq x \leq 0.5$) ceramic powders synthesized with a chemical-coprecipitation and calcination method were sintered at 1873 K for 15 h. Structures of the synthesized powders and sintered ceramics were identified by X-ray diffractometer. The morphologies of ceramic powders were observed by transmission electron microscope. The thermal expansion coefficients and thermal diffusion coefficients of $Sm_xZr_{1-x}O_{2-x/2}$ ceramics were studied with a high-temperature dilatometer and a laser flash diffusivity technique from room temperature to 1673 K. The thermal conductivity was calculated from thermal diffusivity, density and specific heat of bulk ceramics. $Sm_{0.1}Zr_{0.9}O_{1.95}$ ceramics consists of both monoclinic and tetragonal structures. However, $Sm_{0.2}Zr_{0.8}O_{1.9}$ and $Sm_{0.3}Zr_{0.7}O_{1.85}$ ceramics only exhibit a defect fluorite structure. $Sm_{0.4}Zr_{0.6}O_{1.8}$ and $Sm_{0.5}Zr_{0.5}O_{1.75}$ ceramics have a pyrochlore-type lattice. With the increase of Sm_2O_3 content, the linear thermal expansion of $Sm_xZr_{1-x}O_{2-x/2}$ ceramics increases except for $Sm_{0.1}Zr_{0.9}O_{1.95}$. The thermal conductivities of $Sm_xZr_{1-x}O_{2-x/2}$ ceramics ranged from 1.41 at 873 K to 1.86 W m^{-1} K^{-1} at room temperature in a test temperature range of room temperature to 1673 K, and the results can be explained by phonon scattering mechanism.

Keywords: $Sm_xZr_{1-x}O_{2-x/2}$; Coprecipitation-calcination method; Thermal expansion; Thermal conductivity

1. Introduction

The most widely used ceramic material for thermal barrier applications is partially stabilized zirconia due to its relatively low thermal conductivity, relatively high-thermal expansion coefficient and superior high-temperature performance [1–3]. Wu et al. [4] reported that fully dense 7 wt.%Y_2O_3–ZrO_2 ceramics has a thermal conductivity of 3.0 W m^{-1} K^{-1} at room temperature and 2.3 W m^{-1} K^{-1} at 973 K. In order to further enhance thermal stability and reduce thermal conductivity of zirconia-based ceramics at elevated temperatures, significant progress has been made in developing novel low thermal conductive thermal barrier materials with the composition of ZrO_2–Re_2O_3 (Re = rare earth elements) having different rare earth oxide dopants. Thermal conductivity of ceramic materials is both a phonon and photon phenomena dependent on various factors including material structure, operating environment and temperature. It has been reported that multi-component oxide dopants enhance the thermal stability and reduce thermal conductivity by 50% [5]. The reduction in thermal conductivity is due to presence of defect clusters distributed through out the ceramic matrix, which limit the mean free path of both phonons and photons. Next-generation low thermal conductivity zirconia-based thermal barrier coatings are dependent on the use of primary rare earth oxide stabilizers and oxide dopant clusters, such as Y_2O_3, Nd_2O_3 (Gd_2O_3, Sm_2O_3), Yb_2O_3, Sc_2O_3, La_2O_3, etc.

There is increasing demand to use high-temperature structural ceramics with low thermal conductivity for various thermal-insulation applications. Rare-earth zirconates with a general formula of $Re_2Zr_2O_7$, have the lower thermal conductivities in all ceramics [4]. Wu et al. [6] reported that the hot-pressed $Sm_2Zr_2O_7$ ceramics with a relative density of 98% has a thermal conductivity of approximately 1.5 W m^{-1} K^{-1} at 973 K. The thermal conductivity of pressureless-pressed $Sm_2Zr_2O_7$ ceramics with a relative density of 93.4% was 0.88 W m^{-1} K^{-1} at 1073 K [7]. Suresh et al. [8] reported that thermal conductivity of

* Corresponding author. Tel.: +86 451 86414291; fax: +86 451 86414291.
E-mail address: ouyangjh@hit.edu.cn (J.-H. Ouyang).

0272-8842/$34.00
doi:10.1016/j.ceramint.2008.02.016

pressureless-sintered $Sm_2Zr_2O_7$ (90.3% dense) ceramics was approximately 1.45–1.75 W m^{-1} K^{-1} between 673 and 1373 K. The porosity of the materials has a great influence on the thermal conductivity of ceramics, and full dense materials should be prepared in order to compare each other.

Although, thermophysical property of stoichiometric $Sm_2Zr_2O_7$ zirconates has already been reported, there is a paucity of thermophysical property for different ZrO_2–Sm_2O_3 material systems. Previous studies [9–11] discussed the phase structures in ZrO_2–Sm_2O_3 system, but did not deal with thermophysical property of ZrO_2–Sm_2O_3 system. Therefore, it was the purpose of this study to investigate the thermophysical property of ZrO_2–Sm_2O_3 ceramics at elevated temperatures.

2. Experimental procedure

2.1. Preparation and characterization of $Sm_xZr_{1-x}O_{2-x/2}$ ceramics

Samarium oxide powder (Rare-Chem Hi-Tech Co., Ltd., Guangdong, China; purity ≥99.9%) and zirconium oxychloride (Zibo Huantuo Chemical Co. Ltd., Analytical pure) were chosen as the reactants in this investigation. $Sm_xZr_{1-x}O_{2-x/2}$ ($0.1 \leq x \leq 0.5$) ceramic powders were synthesized with a chemical-coprecipitation and calcination method. Samarium oxide powder was first calcined at 1173 K for 2 h to remove adsorptive water and carbon dioxide in air before weighing, and was then weighed and dissolved in diluent nitric acid. Zirconium oxychloride was dissolved in distilled water. These solutions were mixed in appropriate mole ratios ($Sm_xZr_{1-x}O_{2-x/2}$, where $0.1 \leq x \leq 0.5$) and stirred for 30 min. The precursor solution was slowly added under stirring into dilute ammonium hydrate solution with a pH value of 12.5, to obtain gel-like precipitates. These gels were filtered and washed with distilled water for several times until pH = 7, and then washed twice in absolute alcohol. The remains were dried at 373 K for 24 h and then calcined at 1073 K for 5 h for crystallization in air. In order to obtain densified samples of $Sm_xZr_{1-x}O_{2-x/2}$ for the determination of thermophysical properties, the ceramic powders were cold isostatically pressed at 280 MPa, and pressureless-sintered at 1873 K for 15 h in air.

Structures of the synthesized powders were identified by X-ray diffractometer (XRD, Rigaku D/Max-rB, Japan) with Cu Kα radiation at a scan rate of 10°/min. The morphologies of ceramic powders were observed by transmission electron microscope (TEM, JEOL JEM1200, Japan). The phases of the as-sintered bulk ceramics were characterized by X-ray diffractometer with Cu Kα radiation at a scan rate of 4°/min. The relative density of the bulk ceramics was measured by the Archimedes method. The theoretical densities of all samples were calculated using lattice parameters acquired from XRD results and the molecular weight in a unit cell.

2.2. Thermal properties measurements

Thermogravimetry (TG) and differential scanning calorimetry (DSC) of the chemical-coprecipitation products was performed with a simultaneous thermal analysis (STA) (Netzsch STA 449C, Germany) at 10 K/min in an air flow of 30 mL/min in corundum crucibles from room temperature to 1273 K.

The specific heat capacity of $Sm_xZr_{1-x}O_{2-x/2}$ ($0.2 \leq x \leq 0.5$) sintered specimens was measured using disc-shaped specimens, 5 mm in diameter and 0.5 mm in thickness. The specific heat capacity (C_p) was measured from room temperature to 1673 K using simultaneous thermal analysis (STA) (Netzsch STA 449C, Germany) with a heating rate of 20 K/min in air in platinum crucible. The standard material used to calculate specific heat data of the specimens was a certified sapphire.

The thermal diffusivity of the sintered samples was measured employing the laser-flash technique using LFA 427 system (Netzsch Corporation, Germany) from room temperature to 1673 K in an argon gas atmosphere pressure. Cylindrical disc-shaped samples were about 12.7 mm in diameter and about 1.5 mm in thickness. The transient temperature rise of the rear surface of the sample was monitored using an In–Sb sensor. In order to avoid any transmission of the laser beam through the samples and to enhance the optical coupling, an opaque colloidal sprayed graphite suspension was sprayed over the front and rear surface. These pellets were mounted in a graphite sample holder. The values of thermal diffusivity were calculated by using the half time of the maximum temperature increase of the sample rear surface. Measurements were made at 200 K intervals from room temperature to 1673 K. Each sample was measured three times at each temperature. The experimental uncertainty was estimated is ±5%. The thermal conductivity k is given by Eq. (1) with the heat capacity C_p, density ρ and thermal diffusivity λ as follows

$$k = C_p \lambda_\rho \tag{1}$$

As the sintered specimen was not fully dense, the measured thermal-conductivity was corrected for the actual data k_0 using the Eq. (2) [6]:

$$\frac{k}{k_0} = 1 - \frac{4}{3}\varphi \tag{2}$$

where φ is the fractional porosity.

The linear thermal expansion behavior of sintered ceramics using the specimens have dimensions of approximately 4 mm × 4 mm × 20 mm was determined with a high-temperature dilatometer (Netzsch DIL 402C, Germany) from 323 to 1673 K in an argon gas atmosphere. Data was continuously recorded at a heating rate of 4 K/min during heating, and they were corrected using the known thermal expansion of a certified standard alumina.

3. Results and discussion

3.1. TG–DSC thermal analysis and characterization of $Sm_xZr_{1-x}O_{2-x/2}$ ($0.1 \leq x \leq 0.5$) ceramic powders

The TG–DSC patterns of different $Sm_xZr_{1-x}O_{2-x/2}$ ($0.1 \leq x \leq 0.5$) precipitates are shown in Fig. 1. The samples lose weights of 22–27 wt.% from evaporation of water and NH_3

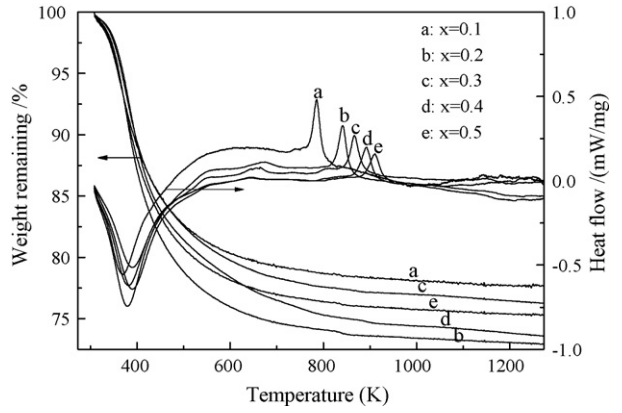

Fig. 1. TG–DSC patterns of $Sm_xZr_{1-x}O_{2-x/2}$ ($0.1 \le x \le 0.5$) precipitates.

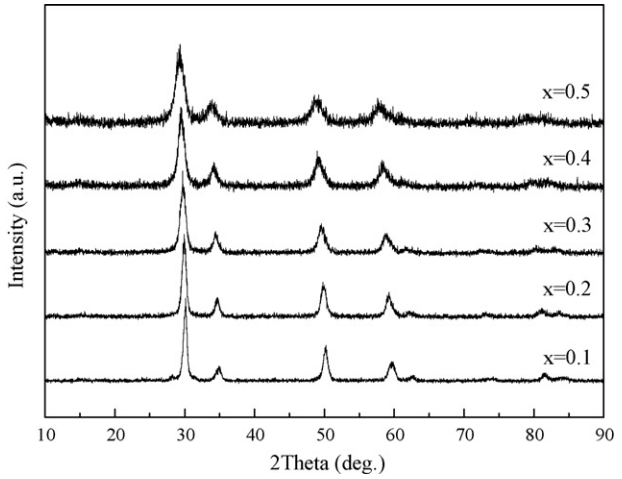

Fig. 2. XRD patterns of $Sm_xZr_{1-x}O_{2-x/2}$ ($0.1 \le x \le 0.5$) ceramic powders.

on heating, depending on their compositions and time of exposure to air after drying. Most of the weight loss takes place below 1073 K. On further heating, weight loss does not exceed 0.5 wt.%. With the increase of temperature and Sm_2O_3 content, $Sm_xZr_{1-x}O_{2-x/2}$ appears exothermic peak at 786, 841, 868, 890 and 908 K, respectively, due to the crystallization of $Sm_xZr_{1-x}O_{2-x/2}$ ceramic powders. It is obvious that crystallization temperature of $Sm_xZr_{1-x}O_{2-x/2}$ ceramic powders gradually increases with the increase of Sm_2O_3 content from $Sm_{0.1}Zr_{0.9}O_{1.95}$ to $Sm_{0.5}Zr_{0.5}O_{1.75}$, which is consistent with the reported crystallization for La_2O_3-ZrO_2 system [12].

Table 1
Relative densities of $Sm_xZr_{1-x}O_{2-x/2}$ ($0.1 \le x \le 0.5$) ceramics

Ceramic materials	Relative densities (%)
$Sm_{0.1}Zr_{0.9}O_{1.95}$	80.1
$Sm_{0.2}Zr_{0.8}O_{1.9}$	95.6
$Sm_{0.3}Zr_{0.7}O_{1.85}$	94.6
$Sm_{0.4}Zr_{0.6}O_{1.8}$	95.1
$Sm_{0.5}Zr_{0.5}O_{1.75}$	97.5

The X-ray diffraction patterns of different $Sm_xZr_{1-x}O_{2-x/2}$ ($0.1 \le x \le 0.5$) ceramic powders are given in Fig. 2. All ceramic powders have wide diffraction peaks, and only exhibit a cubic phase of zirconia, owing to fine grains of ceramic powders. Fig. 3 shows the morphologies of partial $Sm_xZr_{1-x}O_{2-x/2}$ ($x = 0.2$, 0.3) ceramic powders. From TEM observations, $Sm_xZr_{1-x}O_{2-x/2}$ ceramic powders have a uniform particle size of about 20 nm.

The relative densities of sintered $Sm_xZr_{1-x}O_{2-x/2}$ bulk ceramics are shown in Table 1. The relative densities of the $Sm_xZr_{1-x}O_{2-x/2}$ ($0.2 \le x \le 0.5$) bulk ceramics are in the range of 94.6–97.5%, however, $Sm_{0.1}Zr_{0.9}O_{1.95}$ ceramics have a low relative density of 80.1%, which may be due to phase transformation from tetragonal to monoclinic phase on cooling. Fig. 4 reveals the X-ray diffraction patterns of different $Sm_xZr_{1-x}O_{2-x/2}$ ($0.1 \le x \le 0.5$) bulk ceramics. $Sm_{0.1}Zr_{0.9}O_{1.95}$ ceramics consists of both monoclinic and tetragonal structures, and the monoclinic structure is characterized by the presence of typical peaks at 2θ values of about 28° and 31°. However, $Sm_{0.2}Zr_{0.8}O_{1.9}$ and $Sm_{0.3}Zr_{0.7}O_{1.85}$ ceramics only exhibit a defect fluorite structure. $Sm_{0.4}Zr_{0.6}O_{1.8}$ and $Sm_{0.5}Zr_{0.5}O_{1.75}$ ceramics have a pyrochlore-type lattice, which is characterized

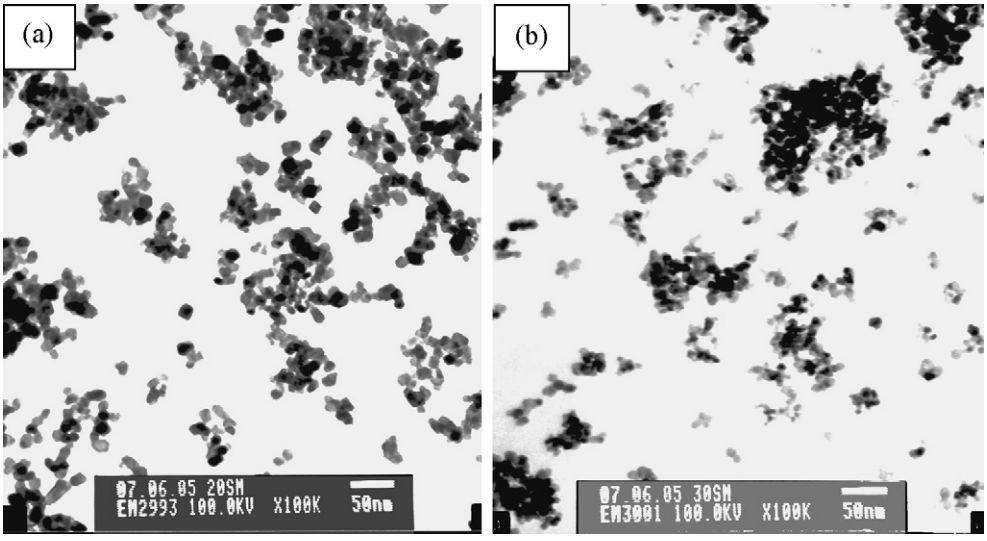

Fig. 3. Morphologies of $Sm_xZr_{1-x}O_{2-x/2}$ ($x = 0.2$, 0.3) ceramic powders: (a) $x = 0.2$; (b) $x = 0.3$.

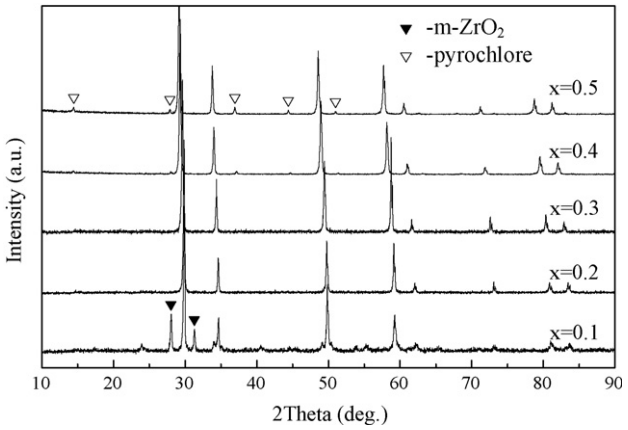

Fig. 4. XRD patterns of $Sm_xZr_{1-x}O_{2-x/2}$ ($0.1 \le x \le 0.5$) ceramics.

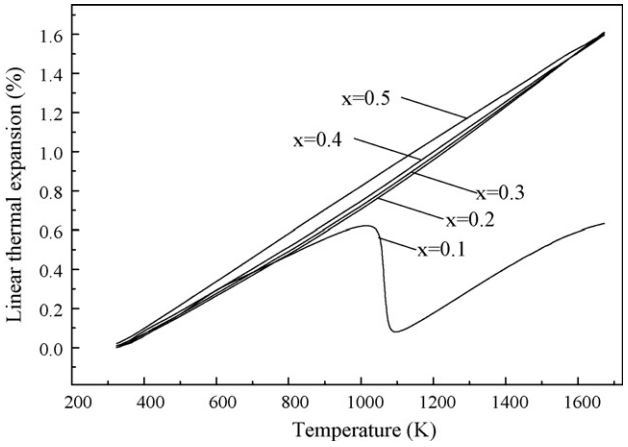

Fig. 5. Measured linear thermal expansion for $Sm_xZr_{1-x}O_{2-x/2}$ ($0.2 \le x \le 0.5$) ceramics as a function of temperature.

by the presence of typical super-lattice peaks at 2θ values of about 14° (1 1 1), 28° (3 1 1), 37° (3 3 1) and 45° (5 1 1) using Cu Kα radiation [13].

3.2. Thermal expansion of $Sm_xZr_{1-x}O_{2-x/2}$ bulk ceramics

The thermal expansions of sintered $Sm_xZr_{1-x}O_{2-x/2}$ bulk ceramics as a function of temperature are presented in Fig. 5. The typical linear expansions are observed in the temperature range of 323–1673 K for $Sm_xZr_{1-x}O_{2-x/2}$ ($0.2 \le x \le 0.5$) ceramics. However, the linear thermal expansion of the $Sm_{0.1}Zr_{0.9}O_{1.95}$ ceramics first increases from 323 to 1015 K, and then decreases from 1015 to 1095 K, and finally increases from 1015 to 1673 K. This is due to the phase transformation from monoclinic to tetragonal phase between 1015 and 1095 K on heating, which is lower than pure zirconia phase transformation temperature (1453–1473 K) [14]. The linear thermal expansion of $Sm_xZr_{1-x}O_{2-x/2}$ ($0.2 \le x \le 0.5$) increases with the increase of temperature, which is a typical characteristic of solid materials as the atom distance increases with the increase of temperature. The linear thermal expansions of the $Sm_xZr_{1-x}O_{2-x/2}$ ($0.2 \le x \le 0.5$) increase with the increasing Sm_2O_3 content from 323 to 1673 K. This can be interpreted as due to weakening binding energy between cation and anion in the crystal structure resulting from oxygen vacancies. The measured thermal expansion of the $Sm_xZr_{1-x}O_{2-x/2}$ ($0.2 \le x \le 0.5$) was fitted as a function of temperature using a cubic polynomial regression ($\Delta L/L(\%) = a + bT + cT^2 + dT^3$), with the fitting parameters as given in Table 2, where T is absolute temperature (K). The beginning temperature (designated as T_0) for calculating thermal expansion is 323 K in this investigation.

Table 2
The fitting parameters of the linear thermal expansion (%) for $Sm_xZr_{1-x}O_{2-x/2}$ ($0.2 \le x \le 0.5$) ceramics as a function of the temperature ($100 \cdot \Delta L/L(\%) = a + bT + cT^2 + dT^3$), 323–1673 K

Composition	a	b ($\times 10^{-3}$)	c ($\times 10^{-7}$)	d ($\times 10^{-11}$)
$Sm_{0.2}Zr_{0.8}O_{1.9}$	−0.28100	0.77599	2.12344	0.14409
$Sm_{0.3}Zr_{0.7}O_{1.85}$	−0.27700	0.77206	2.57096	−2.60462
$Sm_{0.4}Zr_{0.6}O_{1.8}$	−0.27200	0.76617	3.24224	−6.72769
$Sm_{0.5}Zr_{0.5}O_{1.75}$	−0.36800	1.13489	0.96473	−4.12617

Table 3
The fitting parameters of the density for $Sm_xZr_{1-x}O_{2-x/2}$ ($0.2 \le x \le 0.5$) ceramics as a function of the temperature ($\rho(g/cm^3) = a + bT + cT^2 + dT^3$), 323–1673 K

Composition	a	b ($\times 10^{-4}$)	c ($\times 10^{-8}$)	d ($\times 10^{-11}$)
$Sm_{0.2}Zr_{0.8}O_{1.9}$	6.18599	−1.44324	−3.76519	0.13655
$Sm_{0.3}Zr_{0.7}O_{1.85}$	6.22469	−1.45356	−4.66897	0.71084
$Sm_{0.4}Zr_{0.6}O_{1.8}$	6.34101	−1.48196	−5.65323	1.30820
$Sm_{0.5}Zr_{0.5}O_{1.75}$	6.56330	−2.25268	−1.20899	0.75069

The density change by thermal expansion corrected using the following relationship [15] according to data in Fig. 5.

$$\frac{\Delta\rho}{\rho_0} = \frac{1 - (1 + \Delta L/L_0)^3}{(1 + \Delta L/L_0)^3} \quad (3)$$

Table 3 shows the fitted parameters using a cubic polynomial regression as a function of the temperature. In order to compare each other, it was expressed as the relative density, where the density at 323 K was normalized to 1.

3.3. Thermal conductivity of $Sm_xZr_{1-x}O_{2-x/2}$ bulk ceramics

The thermal diffusivities of different $Sm_xZr_{1-x}O_{2-x/2}$ ($0.2 \le x \le 0.5$) bulk ceramics as a function of temperature are shown in Fig. 6. No measurement was made for the $Sm_{0.1}Zr_{0.9}O_{1.95}$ ceramics because of its low relative density (80.1%). The thermal diffusivities exhibited in Fig. 6 are the arithmetic means of every three measurements of identical ceramic materials. The error was derived from the mean standard deviation, however, the error bars in Fig. 6 are smaller than the figure symbols. It can be seen that the thermal diffusivities of $Sm_xZr_{1-x}O_{2-x/2}$ ($x = 0.2, 0.3, 0.4$) decrease with the increase of temperature from room temperature to 1673 K, which suggests a dominant phonon conduction behavior in most polycrystalline materials [16]. But above 1073 K, the thermal diffusivity of $Sm_{0.5}Zr_{0.5}O_{1.75}$ ceramics appreciably increases with the increase of temperature, which is due to the radiative contribution [17].

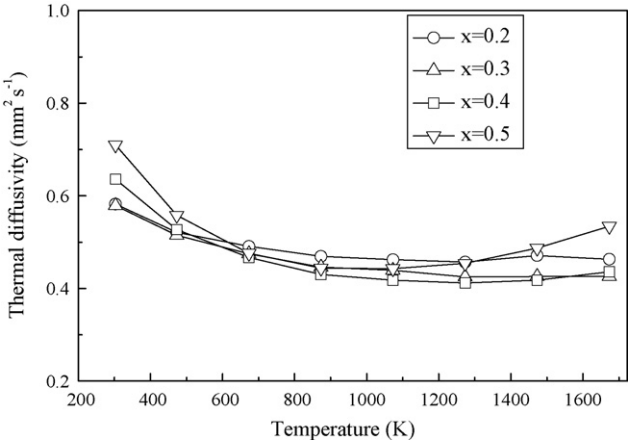

Fig. 6. Thermal diffusivity of $Sm_xZr_{1-x}O_{2-x/2}$ ($0.2 \leq x \leq 0.5$) ceramics as a function of temperature.

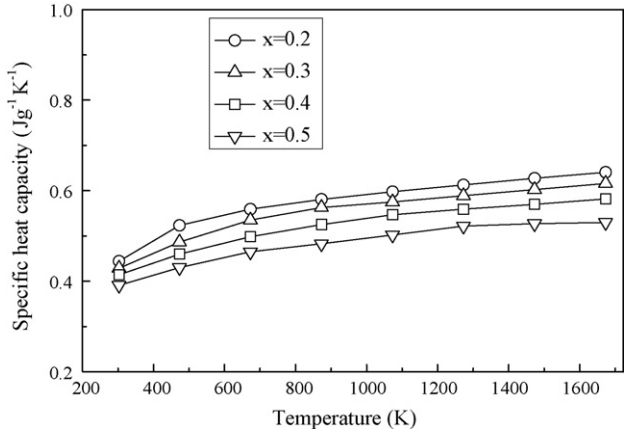

Fig. 7. Specific heat of $Sm_xZr_{1-x}O_{2-x/2}$ ($0.2 \leq x \leq 0.5$) ceramics as a function of temperature.

Fig. 7 shows the specific heat of different $Sm_xZr_{1-x}O_{2-x/2}$ ($0.2 \leq x \leq 0.5$) bulk ceramics as a function of temperature. From all curves illustrated in Fig. 7, the specific heat increases with the increase of temperature. The specific heats of $Sm_xZr_{1-x}O_{2-x/2}$ ceramics increase with the increase of Sm_2O_3 content under identical temperature conditions, which is consistent with the Neumann–Kopp rule [18].

The thermal conductivities of $Sm_xZr_{1-x}O_{2-x/2}$ ($0.2 \leq x \leq 0.5$) bulk ceramics are plotted in Fig. 8 according to the Eq. (1) and the thermal diffusivity values, specific heats and density of different samples. The values in Fig. 8 were corrected to a 100% theoretical density according to Eq. (2) and Table 1. The error bars are omitted because they are smaller than the symbols.

It is well known that the lattice thermal conductivity is proportional to the mean free path of phonon [19]. The substitution of two Zr^{4+} cations with two Sm^{3+} cations is accompanied by the incorporation of one oxygen vacancy, to maintain the electroneutrality of the lattice. The higher the content of Sm_2O_3 is, the more oxygen vacancies are created. The content of Sm_2O_3 is 11.1, 17.6, 25.0, 33.3 mol% in $Sm_xZr_{1-x}O_{2-x/2}$ ($x = 0.2$, 0.3, 0.4, 0.5), respectively. Clearly, the concentration of oxygen vacancies in $Sm_xZr_{1-x}O_{2-x/2}$

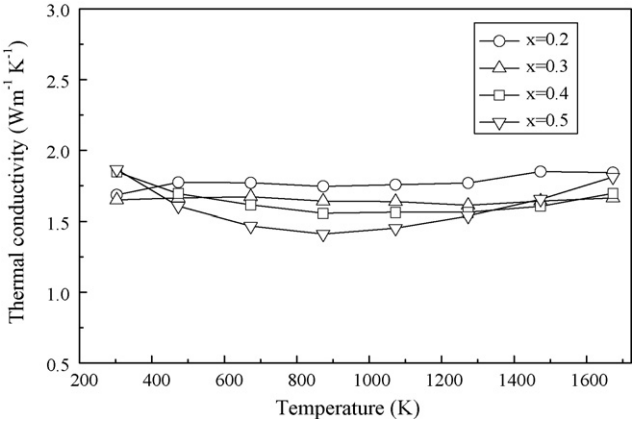

Fig. 8. Thermal conductivity of $Sm_xZr_{1-x}O_{2-x/2}$ ($0.2 \leq x \leq 0.5$) ceramics as a function of temperature.

ceramics increases with the increasing Sm_2O_3 content. Therefore, the thermal conductivity of $Sm_xZr_{1-x}O_{2-x/2}$ ceramics decreases with the increasing Sm_2O_3 content due to the scattering of the phonons by the oxygen vacancies. On the other hand, the phonon mean free path is inverse to the square of the atomic weight difference between the solute (Sm) and host (Zr) cations [20]. Because atomic weights of Zr and Sm are about 91 and 150, respectively, the effective phonon scattering by solute cations is significantly. Therefore, the thermal conductivity of $Sm_xZr_{1-x}O_{2-x/2}$ ceramics decreases with the increasing Sm_2O_3 content due to the scattering of the phonons by the substitutional cation, which is in good agreement with measured values of thermal conductivity below 1273 K. But the thermal conductivity of $Sm_{0.5}Zr_{0.5}O_{1.75}$ ceramic is higher than those of $Sm_xZr_{1-x}O_{2-x/2}$ ($x = 0.2$, 0.3, 0.4) ceramics above 1273 K, which may be attributed to the increased contribution of the radiative component of heat conduction, also known as photon thermal conductivity, with increasing temperature. The thermal conductivity can increase by more than 100% for the very dense specimens because of the increased radiation heat-transfer [17]. The thermal conductivities of $Sm_xZr_{1-x}O_{2-x/2}$ ($0.2 \leq x \leq 0.5$) ceramics were located within the range of 1.41 to 1.86 W m^{-1} K^{-1}, which is clearly lower than those of fully dense 7 wt.%Y_2O_3–ZrO_2 (3.0 at room temperature to 2.3 W m^{-1} K^{-1} at 973 K reported by Wu et al. [4]). Therefore, $Sm_xZr_{1-x}O_{2-x/2}$ ($0.2 \leq x \leq 0.5$) ceramics is a potential candidate for high-temperature thermal-insulation applications.

4. Conclusions

(1) Ceramic powders of $Sm_xZr_{1-x}O_{2-x/2}$ ($0.1 \leq x \leq 0.5$) were synthesized by chemical-coprecipitation and calcination method and sintered into highly dense bulk ceramics.
(2) The $Sm_{0.1}Zr_{0.9}O_{1.95}$ bulk ceramics consists of both monoclinic and tetragonal structures. However, $Sm_{0.2}Zr_{0.8}O_{1.9}$ and $Sm_{0.3}Zr_{0.7}O_{1.85}$ ceramics exhibit a defect fluorite structure. $Sm_{0.4}Zr_{0.6}O_{1.8}$ and $Sm_{0.5}Zr_{0.5}O_{1.75}$ ceramics have a pyrochlore-type lattice.
(3) The linear thermal expansion of $Sm_xZr_{1-x}O_{2-x/2}$ ($0.2 \leq x \leq 0.5$) ceramics increases with the increase of

temperature. The linear thermal expansion of $Sm_xZr_{1-x}O_{2-x/2}$ ($0.2 \leq x \leq 0.5$) ceramics increases with the increasing Sm_2O_3 content under identical temperature conditions.

(4) The thermal conductivities of $Sm_xZr_{1-x}O_{2-x/2}$ ($0.2 \leq x \leq 0.5$) ceramics ranged from 1.41 at 873 K to 1.86 W m^{-1} K^{-1} at room temperature in a test temperature range of room temperature to 1673 K, which is clearly lower than those of fully dense 7YSZ. $Sm_xZr_{1-x}O_{2-x/2}$ ($0.2 \leq x \leq 0.5$) ceramics are potential candidates for high-temperature thermal-insulation applications.

Acknowledgments

The authors would like to thank the financial support by the Program of Excellent Teams in Harbin Institute of Technology (HIT), and the start-up program for high-level HIT faculty returned from abroad.

References

[1] L.B. Chen, Yttria-stabilized zirconia thermal barrier coatings-A review, Surf. Rev. Lett. 13 (5) (2006) 535–544.
[2] S.Q. Guo, Y. Kagawa, Effect of thermal exposure on hardness and Young's modulus of EB–PVD yttria-partially-stabilized zirconia thermal barrier coatings, Ceram. Int. 33 (3) (2007) 263–270.
[3] S.Q. Guo, Y. Kagawa, Isothermal and cycle properties of EB-PVD yttria-partially-stabilized zirconia thermal barrier coatings at 1150 and 1300 °C, Ceram. Int. 33 (3) (2007) 373–378.
[4] J. Wu, N.P. Padture, P.G. Klemens, M. Gell, E. Garcia, P. Miranzo, M.I. Osendi, Thermal conductivity of ceramics in the ZrO_2–$GdO_{1.5}$ system, J. Mater. Res. 17 (12) (2002) 3193–3200.
[5] D.M. Zhu, R.A. Miller, Development of advanced low conductivity thermal barrier coatings, Int. J. Appl. Ceram. Tec. 1 (1) (2004) 86–94.
[6] J. Wu, X.Z. Wei, N.P. Padture, P.G. Klemens, M. Gell, E. Garcia, P. Miranzo, M.I. Osendi, Low-thermal-conductivity rare-earth zirconates for potential thermal-barrier-coating applications, J. Am. Ceram. Soc. 85 (12) (2002) 3031–3035.
[7] J.D. Wang, W. Pan, Q. Xu, K. Mori, T. Torgoe, Thermal conductivity of the new candidate materials for thermal barrier coatings, Key Eng. Mater. 280-283 (2005) 1503–1506.
[8] G. Suresh, G. Seenivasan, M.V. Krishnaiah, P.S. Murti, Investigation of the thermal conductivity of selected compounds of lanthanum, samarium and europium, J. Alloy. Compd. 269 (1998) L9–L12.
[9] M. Yashima, K. Ohtake, M. Kakihana, H. Arashi, M. Yoshimura, Determination of tetragonal-cubic phase boundary of $Zr_{1-x}R_xO_{2-x/2}$ (R = Nd, Sm, Y, Er and Yb) by Raman scattering, J. Phys. Chem. Solids. 57 (1) (1996) 17–24.
[10] E.R. Andrievskaya, L.M. Lopato, Influence of composition on the T → M transformation in the systems ZrO_2–Ln_2O_3 (Ln = La, Nd, Sm, Eu), J. Mater. Sci. 30 (10) (1995) 2591–2596.
[11] Y. Tabira1, R.L. Withers, Structure crystal chemistry as a function of composition across the wide range nonstoichiometric $(1-\varepsilon)$ $ZrO_2{\cdot}\varepsilon SmO_{1.5}$, 0. 38<$\varepsilon$<0.55, oxide pyrochlore system, J. Solid. State. Chem. 148 (2) (1999) 205–214.
[12] S.V. Ushakov, C.E. Brown, A. Navrotsky, Effect of La and Y on crystallization temperatures of hafnia and zirconia, J. Mater. Res. 19 (3) (2004) 693–696.
[13] B.P. Mandal, A.K. Tyagi, Preparation and high temperature-XRD studies on a pyrochlore series with the general composition $Gd_{2-x}Nd_xZr_2O_7$, J. Alloy. Compd. 437 (2007) 260–263.
[14] P.M. Kelly, C.J. Wauchope, The tetragonal to monoclinic martensitic transformation in zirconia, Key. Eng. Mater. 153–154 (1998) 97–124.
[15] D.J. Kim, Y.S. Kim, S.H. Kim, J.H. Kim, J.H. Yang, Y.W. Lee, H.S. Kim, The linear thermal expansion and the thermal diffusivity measurements for near-stoichiometric (U, Ce) O_2 solid solutions, Thermochim. Acta 441 (2006) 127–131.
[16] G.E. Youngblood, R.W. Rice, R.P. Ingel, Thermal diffusivity of partially and fully stabilized (yttria) zirconia single crystals, J. Am. Ceram. Soc. 71 (4) (1988) 255–260.
[17] N.P. Mansal, D.M. Zhu, Effects of doping on thermal conductivity of pyrochlore oxides for advanced thermal barrier coatings, Mater. Sci. Eng. A 459 (2007) 192–195.
[18] J. Leitner, C. Pavel, S. David, S. Ales, A. Petr, Estimation of heat capacities of solid mixed oxides, Thermochim. Acta 395 (2003) 27–46.
[19] R. Mevrela, J.C. Laizet, A. Azzopardi, B. Leclercq, M. Poulain, O. Lavigne, D. Demange, Thermal diffusivity and conductivity of $Zr_{1-x}Y_xO_{2-x/2}$ (x = 0, 0.084 and 0.179) single crystals, J. Eur. Ceram. Soc. 24 (10) (2004) 3081–3089.
[20] P.G. Klemens, Phonon scattering by oxygen vacancies in ceramics, Physica B 263–264 (1999) 102–104.